NANO · MICRO small
www.small-journal.com

Lipopeptide-Based Nanosome-Mediated Delivery of Hyperaccurate CRISPR/Cas9 Ribonucleoprotein for Gene Editing

*Trung Thanh Thach, Do Hyun Bae, Nam Hyeong Kim, Eun Sung Kang, Bok Soo Lee, Kayoung Han, Minsuk Kwak, Hojae Choi, JiYoung Nam, Taegeun Bae, Minah Suh, Junho K. Hur, and Yong Ho Kim**

A transient cytosolic delivery system for accurate Cas9 ribonucleoprotein is a key factor for target specificity of the CRIPSR/Cas9 toolkit. Owing to the large size of the Cas9 protein and a long negative strand RNA, the development of the delivery system is still a major challenge. Here, a size-controlled lipopeptide-based nanosome system is reported, derived from the blood-brain barrier-permeable dNP2 peptide which is capable of delivering a hyperaccurate Cas9 ribonucleoprotein complex (HypaRNP) into human cells for gene editing. Each nanosome is capable of encapsulating and delivering ≈2 HypaRNP molecules into the cytoplasm, followed by nuclear localization at 4 h post-treatment without significant cytotoxicity. The HypaRNP thus efficiently enacts endogenous eGFP silencing and editing in human embryonic kidney cells (up to 27.6%) and glioblastoma (up to 19.7% frequency of modification). The lipopeptide-based nanosome system shows superior delivery efficiency, high controllability, and simplicity, thus providing biocompatibility and versatile platform approach for CRISPR-mediated transient gene editing applications.

The RNA-guided CRISPR/Cas9 tool kit (clustered regularly interspaced short palindromic repeats/CRISPR associated protein 9) for genome engineering is being widely used, for various applications from basic research to the development of novel therapeutics.[1] While the genome editing tool holds tremendous promise for biomedical applications, the unstable and large size of the CRISPR/Cas9 system have been one of the major challenges of its effective intracellular delivery.[2] Additionally, the target specificity of the CRISPR/Cas9 system has also been a critical issue.[2a,3] For permanently modifying genomic DNA using genome editing techniques, the specific and one-time effect is of utmost importance. Previously, genes encoding the CRISPR/Cas9 components, namely, the Cas9 protein and guide

Dr. T. T. Thach, N. H. Kim, E. S. Kang, Dr. B. S. Lee, Dr. M. Kwak, H. J. Choi, J. Nam, Prof. Y. H. Kim
SKKU Advanced Institute of Nanotechnology (SAINT)
Sungkyunkwan University
South Suwon 16419, Korea
E-mail: yhkim94@skku.edu

D. H. Bae, Prof. Y. H. Kim
Department of Biomedical Engineering
Sungkyunkwan University
Suwon 16419, South Korea

K. Han, Prof. M. Suh
Center for Neuroscience Imaging Research (CNIR)
Institute for Basic Science (IBS)
Sungkyunkwan University
Suwon 16419, South Korea

T. Bae
Department of Medicine
Graduate School
Kyung Hee University
Seoul 02447, South Korea

Prof. M. Suh
Department of Nano Engineering
Sungkyunkwan University
Suwon 16419, South Korea

Prof. J. K. Hur
Department of Pathology
College of Medicine
Kyung Hee University
Seoul 02447, South Korea

Prof. J. K. Hur
Department of Biomedical Science
Graduate School
Kyung Hee University
Seoul 02447, South Korea

Prof. Y. H. Kim
Biomedical Institute for Convergence at SKKU (BICS)
Sungkyunkwan University
Suwon 16419, South Korea

The ORCID identification number(s) for the author(s) of this article can be found under https://doi.org/10.1002/smll.201903172.

DOI: 10.1002/smll.201903172

RNA from *Streptococcus pyogenes* (SpCas9), were delivered via plasmids using either lipofectamine or by viral vectors, which prolonged their expression, thus raising off-target effects and toxicity.[2b,4] To minimize the off-target effects, one of the more straightforward approaches is the delivery of the Cas9:sgRNA ribonucleoprotein complex (RNP) in vitro and in vivo.[3b] This approach directly delivers high levels of the genome editing RNP machinery that functions immediately without transcription and translation. Moreover, the RNP complex is transient which means that it is rapidly cleared in cells, resulting in a "fast on, fast off" mode with high efficiency, specificity, and low toxicity compared to the strategies involving viral delivery of genes coding Cas9:sgRNA.[2b,5] The delivery of RNP using cationic lipid-induced genomic modification with approximately tenfold higher specificity compared to plasmid transfection.[5b] However, as the widely used SpCas9 is a large multidomain protein (1368 aa, ≈10 nm diameter) with a high positive charge and a long negative strand of sgRNA,[6] several aspects of developing effective delivery systems for RNPs remain a challenge that is continuously being tackled. The application of gold nanoparticles,[5a,7] black phosphorus nanosheets,[8] or metal-coordination frameworks[9] have demonstrated their utility as efficient RNP delivery platforms. However, the aforementioned systems are limited by large size (over 100 nm), low levels of endosomal escape, usage of nonbiodegradable materials and metals that results in prevention of intracellular uptake and RNP release, and incensement of toxicity problems.

Lipopeptides are amphiphilic molecules that can self-assemble to form peptide-functionalized nanostructures. Lipopeptide-based nanoparticles are well-suited for intracellular delivery of macromolecules, which are encapsulated in the solvent-filled cavity.[10] To further improve the delivery efficiency, they can be modified to target cellular membrane by introducing appropriate components. Here, we developed a size-controlled delivery system derived from dNP2 lipopeptide, hereafter called nanosome. dNP2 is a tandem repeat of the blood-brain barrier-permeable peptide (KIKKVKKKGRK), which is highly efficient in in vitro and in vivo deliveries, including to brain tissue without significant toxicity.[11] The intracellular delivery of dNP2 mainly utilizes lipid raft-mediated endocytosis upon heparan sulfate interaction, resulting in highly efficient delivery and endosomal escape in the cytosol.[11a,12]

As previous report showed that the hyperaccurate SpCas9 (HypaCas9) variant efficiently and specifically mediated gene editing better than WT protein by reducing the relative affinity to the target DNA,[13] we performed site-direct mutagenesis to obtain a HypaCas9 variant with seven point-mutations (K848A, K1003A, R1060A, N497A, R661A, Q695A, and Q926A) in SpCas9 WT (**Figure 1**a and Figure S1, Supporting Information). To use HypaCas9 for gene editing in mammalian cells, we further inserted the SV40 nuclear localization signal (NLS, PKKKRKV) at the C-terminus with flexible GGS linker to enrich in mammalian cell nuclei (Figure 1a). Successful overexpression and purification of Cas9 via the recombinant His-MBP tag were confirmed using fast protein liquid chromatography (FPLC) and sodium dodecyl sulfate (SDS)-PAGE (Figure S2a–d, Supporting Information). Furthermore, to monitor HypaCas9:sgRNA ribonucleoprotein complex (HypaRNP) localization, we labeled HypaCas9 with Cy3 maleimide via two solvent-exposed cysteine residues on the protein (C80 and C574) (Figure S2c,d, Supporting Information). Cy3-labeled HypaCas9 did not hamper the protein folding and the nuclease activity compared to free HypaCas9 as was evident from the results of circular dichroism and DNA cleavage assay, respectively (Figure S2e,f, Supporting Information). The results showed that our labeled protein is suitable for use similar to free protein. Our key goal was to generate size-controlled lipopeptide-based nanosomes derived from dNP2 with a cavity suitable to encapsulate and directly deliver HypaRNP into human cells for gene editing. Towards this purpose, we first chemically synthesized a blood-brain barrier-permeable dNP2 peptide using the solid-phase peptide chemistry. To generate dNP2 lipopeptide variants, we next conjugated the peptide to different types of saturated fatty acids including caprylic or octanoic acid (C8:0), capric or decanoic acid (C10:0), and myristic or tetradecanoic acid (C14:0) through a peptide bond. Successful synthesis and purification of the lipopeptides were confirmed using reverse-phase high-performance liquid chromatography (HPLC), followed by matrix-assisted laser desorption/ionization-time-of-flight (MALDI-TOF) analysis (Figure S3a–c, Supporting Information). Analyses of the final products showed the corrected molecular mass for each lipopeptide with purity level over 95% (Figure S3a–c, Supporting Information). To check the capacity of the nanosomes formed from the designed dNP2 lipopeptides for further cell-treatment, we examined the hydrodynamic diameters of these lipopeptide-based nanosomes using dynamic light scattering (DLS). The analysis showed that at a lipopeptide concentration of 50×10^{-6} M, the diameters of the C8dNP2 and C10dNP2 nanosomes were ≈27.2 and ≈30 nm, respectively; the longer lipopeptide, C14dNP2, was over 500 nm (Figure S4a and Table S2, Supporting Information). Consistently, the further transmission electron microscopy (TEM) analysis revealed that the C14dNP2 lipopeptide was aggregated or unable to form nanosomes, whereas C8dNP2 was able to form homologous nanosomes better than the C10dNP2 (Figure S4b, Supporting Information). Alternatively, the 3D structure and length of the free dNP2 lipopeptide were theoretically modeled and calculated using *Phyre*[14] and *PyMol*,[15] respectively. The length of the free C8dNP2 lipopeptide was estimated to be ≈2.8 nm, suggesting that the lipopeptide-based nanosomes have a capacity to encapsulate HypaRNP, which is ≈10 nm of size (Figure 1b–d and Figure S1, Supporting Information). Therefore, we selected C8dNP2-based nanosomes for HypaRNP encapsulation experiments. To investigate the HypaRNP encapsulation condition using the C8dNP2-based nanosomes with minimal lipopeptide concentration, we purified the RNP complex using a size exclusion column (Figure S2a–d, Supporting Information) and then encapsulated 0.5×10^{-6} M of RNP in nanosomes using different C8dNP2 lipopeptide concentrations. The hydrodynamic diameter assessed using DLS indicated that the diameter of HypaRNP was ≈10.0 nm (Table S2, Supporting Information), which is consistent with the size predicted from the atomic structure (Figure S1, Supporting Information) and TEM data (Figure S4c, Supporting Information). The RNP might not stably be encapsulated in the nanosomes formed by 12.5×10^{-6} M C8dNP2 (ratio 25:1) with the low and broad size distribution (**Figure 2**a). We hypothesized that the 25:1 molar ratio of the lipopeptide to RNP is not enough for

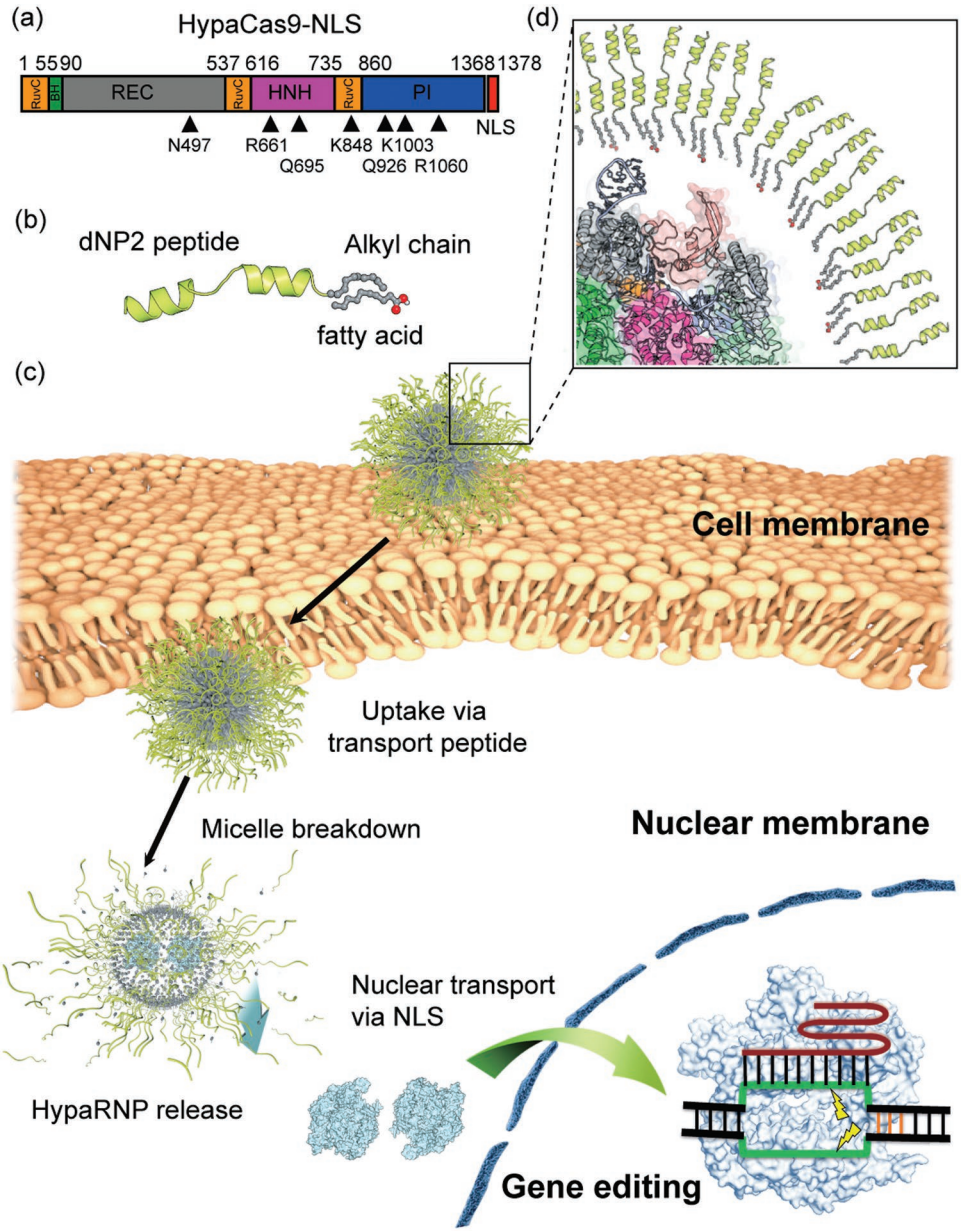

Figure 1. Schematic illustration displaying the formation and intracellular delivery of HypaCas9 RNP-encapsulated nanosome for gene editing. a) HypaCas9-NLS engineering. Residue numbers for the boundaries of domains and the construct are displayed. Residues mutated in this study are indicated by filled triangles. b) Structure model of dNP2 lipopeptide and fatty acid. c,d) Encapsulating the HypaCas9 RNP within dNP2 lipopeptide-based nanosomes. The blood-brain barrier-permeable dNP2 peptide may facilitate direct transcytosis and release of the HypaRNP for gene editing in human cells. NLS, SV40 nuclear localization signal peptide.

nanosome proportion to encapsulate the RNP. Hence, we next examined the 50:1 and 100:1 ratio with nanosome concentrations of 25 and 50 $\times$ 10^{-6} M, respectively. DLS data showed the diameter of the C8dNP2/RNP ratio of (50:1) and (100:1) were ≈35.2 and ≈40.5 nm, respectively; which is considered a potential condition for complete encapsulation of HypaRNP by the C8dNP2-based nanosomes (Figure 2a, Table S2, Supporting Information). Measuring zeta potential showed that the positively charged HypaRNP-encapsulated nanosomes were 37.1 ± 7.8 mV compared to 33.6 ± 6.9 mV of the free nanosomes and 0.5 ± 5.3 mV of HypaRNP indicating that the positive nanosome system would facilitate the intracellular delivery of HypaRNP (Table S2, Supporting Information). Further TEM data also consistently showed the highly homologous morphology of the RNP-encapsulated nanosomes in the 50:1 ratio with the size of ≈35 nm (Figure 2b). To minimize the amount of lipopeptide usage, we selected 25 $\times$ 10^{-6} M of C8dNP2-based nanosomes for further experiments. UV–visible spectrophotometric data indicated that the Cy3 fluorescence decreased significantly by 64 ± 12% in the encapsulated RNP-based nanosomes for 4 h at least, but not in the unencapsulated mixture (free Cy3RNP and lipopeptide), indicating that

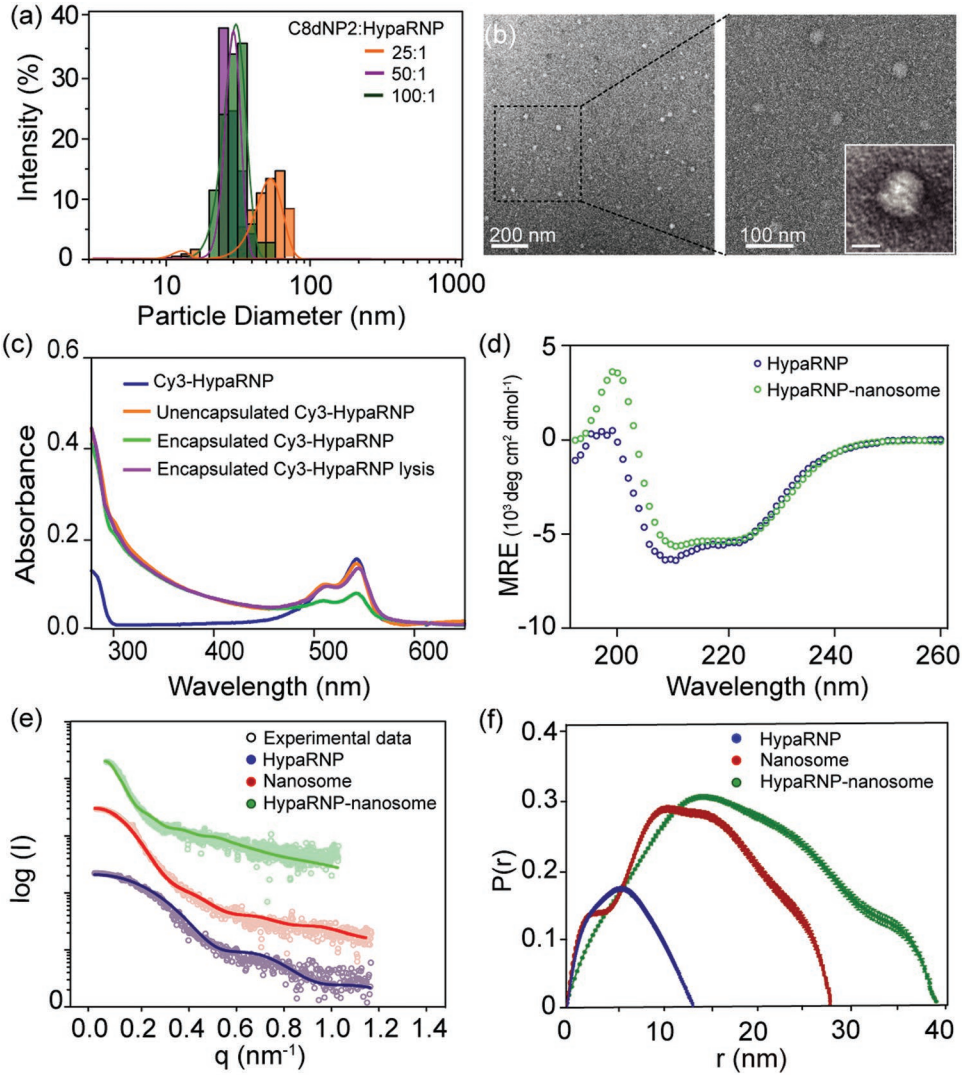

Figure 2. The HypaCas9 RNP-encapsulated nanosome. a) Distribution of hydrodynamic diameter of HypaRNP-encapsulated C8dNP2-nanosomes (HypaRNP-nanosome). A constant amount of RNP was encapsulated by C8dNP2-based nanosomes with various molar ratios. b) Representative TEM images of RNP-encapsulated C8dNP2-based nanosomes. Scale bar, 20 nm. c) UV–visible spectra showing the encapsulation of Cy3-RNP within C8dNP2-based nanosomes. Cy3 absorbance signal is significantly decreased in the encapsulated RNP, but recovered after lysis compared to free Cy3-RNP or unencapsulated Cy3-RNP. d) CD spectra of free HypaRNP and HypaRNP-nanosome. Either buffer or the nanosome was used as a baseline signal for the RNP or RNP-nanosome, respectively. e) Small-angle X-ray scattering measurements in a globular fitting curve for HypaRNP, nanosome, and HypaRNP-nanosome. f) Pair distribution function derived from SAXS measurements of HypaRNP, C8dNP2 nanosome, and HypaRNP-nanosome.

the HypaRNP is stably encapsulated within the C8dNP2-based nanosome (Figure 2c and Figure S5, Supporting Information). The encapsulation was validated by lysing of the nanosomes using protease K, in which the Cy3 intensity was recovered similarly to the unencapsulated ones (Figure 2c). Importantly, the CD data showed a similar ratio of the secondary structure of the RNP without and with the nanosome encapsulation (Figure 2d and Table S3, Supporting Information), suggesting the C8dNP2-based nanosome system did not disrupt the RNP structure. Together, these data suggested that HypaRNP is suitably encapsulated in the lipopeptide-based nanosome system without loss of Cas9 nuclease activity. We further explored the shape and molecular mass of C8dNP2-based nanosome system in aqueous phase using small-angle X-ray scattering (SAXS) measurements. In the small-angle region of the scattering vector $q < 0.1$ Å^{-1}, the experimental scattering profile followed the q^{-1} power law, corresponding to the globular shape (Figure 2e). The pair distribution functions, ($P(r)$), displayed a bell-shape, indicating a characteristic of the globular shape with a maximum interatomic distance, D_{max} of 11.9 nm (HypaRNP), 28.7 nm (nanosome) and 39.1 nm (RNP-encapsulated nanosome) (Figure 2f and Table S4, Supporting Information). The radius of gyration R_g determined from Guinier plots was in good agreement with that from $P(r)$, supporting the monodisperse state of the sample during SAXS measurements (Table S4, Supporting Information). The molecular mass of the RNP, nanosome, or RNP-nanosome was calculated via the absolute scattering intensity using bovine serum albumin (BSA)

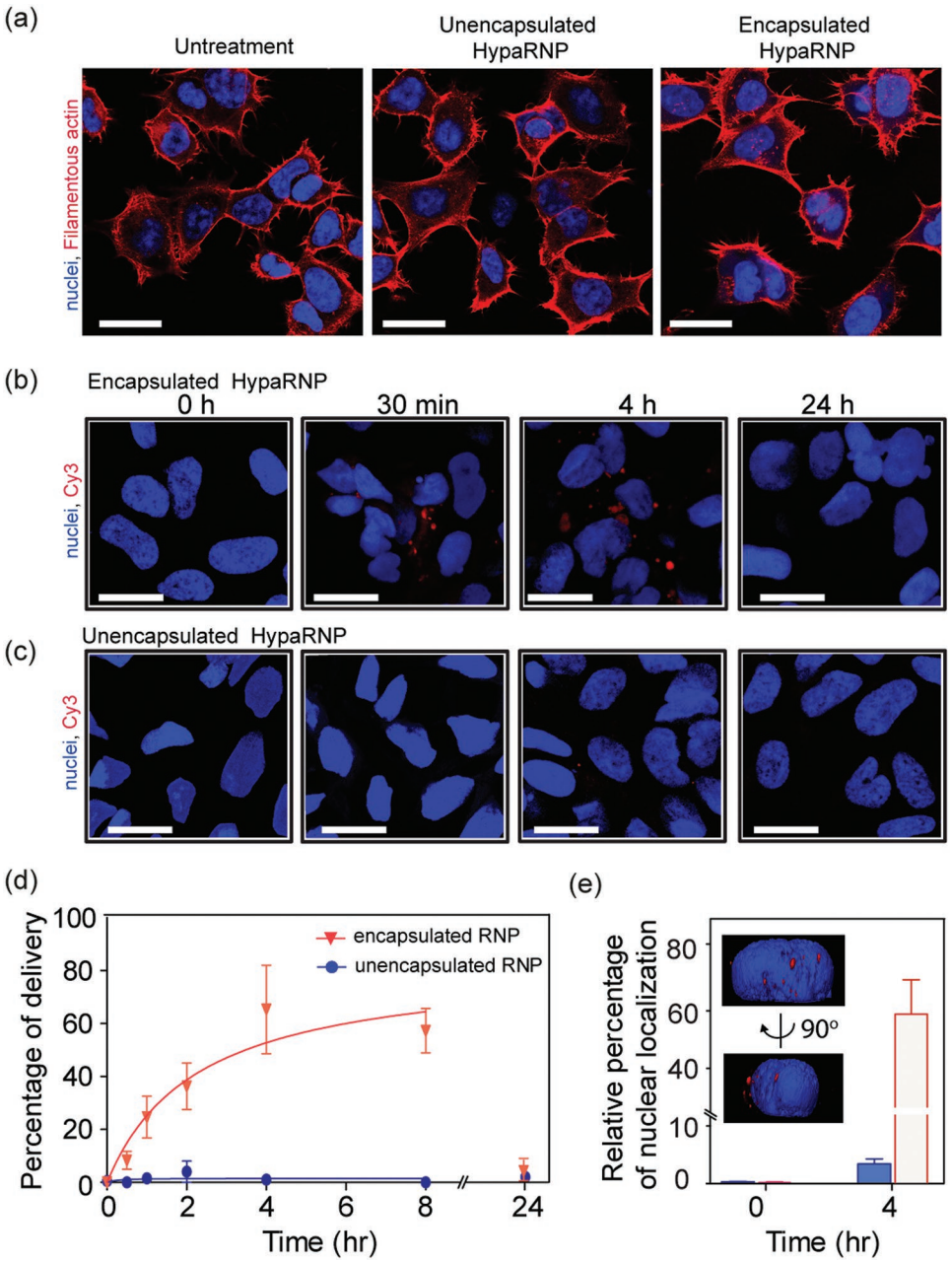

Figure 3. Intracellular delivery of the Cy3-HypaCas9 RNP complex in human embryonic kidney cells via C8dNP2-based nanosomes. a) Cellular morphology was probed by filamentous actin (red). Time tracking of cellular uptake of b) encapsulated and c) unencapsulated HypaRNP-nanosomes. Cy3-labled HypaRNP was used to probe the HypaRNP delivery. d) Percentage of intracellular delivery of the HypaRNP mediated by the nanosomes. Zero represents the beginning of the treatment. e) Relative percentage of nuclear localization of HypaRNP. Representative confocal *z*-stacking 3D images show the location of HypaRNP within the nucleus. Scale bar, 20 µm.

scattering as a standard. The RNP-nanosome showed a mass increase of 339 kDa compared to nanosome only, suggesting that each nanosome may contain ≈2 RNP molecules (Table S4 (Supporting Information) and Figure 1c).

We sought to access the nanosome-mediated intracellular delivery of HypaRNP. To the end, we generated eGFP-reporter HEK cells, which harbored an eGFP gene integrated into the host genome. We harvested the eGFP-reporter HEK cells, which stably express the eGFP protein using flow cytometry (Figure S6, Supporting Information). The cytotoxicity of our delivery system was then examined based on the measurement of cell viability. We found no significant toxicity below 50×10^{-6} M concentration of the C8dNP2-based nanosome (Figure S7a–c, Supporting Information). Cell viability was reduced by ≈20–70% in the concentration range of 50–100 $\times$ 10^{-6} M (Figure S7a–c, Supporting Information). Consistently, the cellular morphology was not influenced by the treatment with 0.5×10^{-6} M of HypaRNP-unencapsulated or encapsulated nanosome

(25×10^{-6} M) compared to untreated cell population (**Figure 3**a). We anticipated that highly efficient gene editing would be achieved by effective RNP delivery. To assess the efficiency of delivering HypaRNP by the C8dNP2-based nanosomes, we treated eGFP-reporter HEK cells in Dulbecco's modified Eagle's medium with our HypaRNP-nanosome system. The efficiency of cellular uptake of Cy3-HypaRNP was probed through Cy3 fluorescence. The cellular uptake and release of HypaRNP were shown to increase from 30 min post-treatment, and the process was nearly complete at 4 h with 70 ± 11% efficiency. The Cy3 fluorescence was then cleared in the cells at 24 h. On the other hand, the fluorescence was not observed in cells treated with either free HypaRNP or unencapsulated Cy3-HypaRNP (Figure 3b–d and Figure S8, Supporting Information). Importantly, we observed that RNP also rapidly reached cell nuclei after transcytosis (Figure S8, Supporting Information). To validate the nuclear localization of the RNP, we performed Z-stacking to construct a 3D image of the nuclei at 4 h post-treatment. Our 3D images and *Z*-axis sections revealed that the Cy3-HypaRNP is specifically localized in most nuclei treated with the RNP-nanosomes (58 ± 13%), while unencapsulated Cy3-HypaRNP showed nonspecific spatial distribution (Figure 3e and Figure S9, Supporting Information).

To subsequently investigate the nanosome-based delivery system could efficiently mediate genome modification in the human cells; we targeted the endogenous eGFP gene in our eGFP-reporter HEK cell system (Figure 1c). Delivery of CRIPSR/Cas9 system to nucleus induces double-strand breaks (DSB) at the target genomic loci at the eGFP gene, and the repair of the DSB by cellular system results in insertion/deletion (indels) mutations at the DNA cleavage point, which may abrogate the expression of the reporter eGFP.[16] The HEK cells were treated twice sequentially with either unencapsulated HypaRNP or HypaRNP-encapsulated nanosomes, and subsequently incubated for 3 days. The eGFP fluorescence was then analyzed using either confocal microscopy or flow cytometry. We observed that the unencapsulated and encapsulated HypaRNP-nanosome treatment reduced the eGFP expression by 7 ± 5% and 37 ± 18%, respectively, compared to the untreated control (**Figure 4**a and Figure S10a, Supporting Information). Further flow cytometry analysis showed that the average frequency of eGFP-negative cells in the population was 17.2 ± 2.6% for the nanosome-mediated treatment with reference to untreated cells (Figure 4b,c and Figure S10b, Supporting Information). Meanwhile, the treatment with unencapsulated HypaRNP resulted in slight and nonsignificant increase of the eGFP-negative population, suggesting the importance of nanosome-mediated HypaRNP delivery. The flow cytometry data also revealed the frequency of disruption of the eGFP gene modification by the nanosome-mediated methods was higher compared to that obtained using lipofectamine 2000 (9.1 ± 1.5%) or CRISPRMAX (11.4 ± 1.8%) (Figure 4c and Figure S10b, Supporting Information). To further access the target gene modification rate, we isolated genomic DNA and PCR amplified the eGFP genomic locus using specific set of primers (Table S1, Supporting Information). The amplified PCR product was treated with mismatch-sensitive T7 endonuclease 1 (T7E1). Results of the T7E1 assay showed an indel mutation frequency up to 27.6% (Figure 4d) that is slightly higher than that of SpCas9WT (26.1%) (Figure S10c, Supporting Information). The gene editing of the HypaRNP-encapsulated nansomes was further validated in eGFP-reporter human glioblastoma cells with ≈20% of indel mutation frequency (Figure S11 (Supporting Information) and Figure 4e). The frequency level achieved by lipopeptide-based nanosome-mediated delivery is significantly higher compared to previous systems such as SpCas9WT-conjugated poly-arginine (≈6%),[17] plasmid encoding SpCas9WT and sgRNA (≈7%),[18] gold nanoparticle (≈11%);[6] and comparable to delivery platforms of black phosphorus nanosheets (≈32%)[8] or Zeolitic Imidazolate frameworks (≈30%).[9] Collectively, our data showed that the HypaRNP-delivered nanosomes efficiently mediated editing of the endogenous gene in human cells.

In conclusion, we successfully generated and characterized a C8dNP2 lipopeptide-based nanosome system that efficiently delivered hyperaccurate SpCas9 RNP complex into human cells. Our system showed high efficiency (70 ± 11%) of intracellular delivery in HEK cells at 4 h post-treatment. Further analysis showed the HypaRNP-induced endogenous eGFP gene editing frequency of indel mutations were up to 27.6% in HEK and 19.7% in human glioblastoma cells. Together, we conclude that the lipopeptid-based nanosome-mediated system efficiently delivered HypaRNP for endogenous editing, which will contribute to broaden the scope for transient gene editing technology.

Experimental Section

Lipopeptide Synthesis, Purification, and Characterization: Peptides were synthesized using Fmoc-solid-phase-peptide-synthesis (SPPS) on a Libertyblue automatic microwave synthesized system. The mixture of 5:4.9:10:1 molar ratio of amino acid: *N*,*N*-diisopropylcarbodiimide (DIC): ethyl 2-cyano-2-(hydroxyimino)acetate (Oxyma): resin was used for each coupling reaction. To generate the lipopeptide, aliphatic chains were conjugated to peptides by coupling of octanoic acid (8C), decanoic acid (10C), or myristic acid (14C) to the *N*-terminus of the peptide. The Fmoc deprotection reaction was performed using piperidine: dimethylformamide (DMF) (ratio 20:80 v/v). The products finally were cleaved from the resin using a mixture of trifluoroacetic acid (TFA), triisopropylsilane (TIS), and deionized water (DI water) (95:2.5:2.5 v/v) for 2 h at ambient temperature, and subsequently precipitated using cold anhydrous diethyl ether. The products were loaded on C4 column (Waters XBridgeTM, Massachusetts, USA) and purified using reverse-phase HPLC (Waters Quaternary Gradient Module 2545) and gradients of mobile phase A (0.1% TFA solution) and mobile phase B (90% of solution of 0.1% TFA in ACN (Acetonitrile)). The purity and molecular mass of the fractions were subsequently confirmed using MALDI-TOF mass spectra with flex control 1.01 (Brucker Ultraflex III, Germany).

Preparation of HypaRNP-Encapsulated Nanosome: For lipopeptide-based nanosome formation, the working molarity was determined by screening different concentrations. For generating the HypaRNP-encapsulated nanosome, the lyophilized lipopeptide was dissolved in PBS buffer, pH 7.4, supplemented with 5×10^{-3} M $MgCl_2$, 10% glycerol, and 0.2×10^{-6} M saturated fatty acid. The RNP-encapsulated nanosome was prepared by sonication with 20% amplitude for 15 min, pulse/pause of 2 s/2 s at 4 °C (Sonics, UK), simultaneously added HypaRNP. The solution was subsequently filtered through 0.2×10^{-6} M Whatman filter membrane (Merck, MA, USA) and immediately used for treatment. The encapsulation efficiency was monitored based on the absorbance spectra of the Cy3-labled Cas9 per the following formula: efficiency (%) = [(unencapsulated − encapsulated)/unencapsulated Cy3HypaRNP] × 100. The spectra were measured using UV–visible spectroscopy (Cary 8454 UV-Vis, Aglient Technologies, CA, USA)

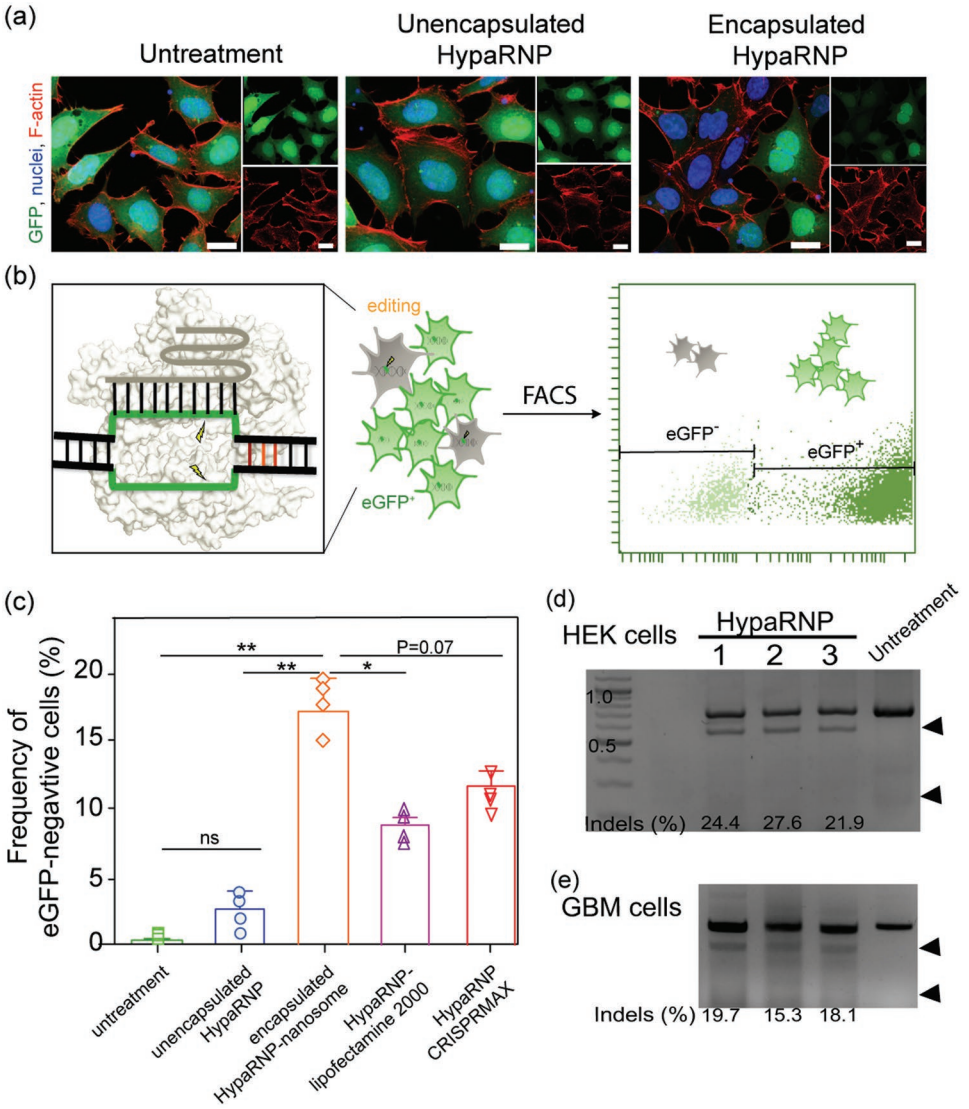

Figure 4. Nanosome-mediated delivery of HypaRNP induces endogenous gene modification. a) Lipopeptide-based nanosome-mediated intracellular delivery of HypaRNP targets eGFP gene modification, thus reducing eGFP protein expression. b) Schematic representation of the flow cytometric analysis of eGFP-negative cells containing RNP-induced indel mutations. c) The comparison of the frequency of eGFP-negative cell population calculated from flow cytometry. The frequency of nanosome-mediated RNP delivery-induced indel mutations on the eGFP target gene in d) HEK and e) glioblastoma cells. Arrows indicate the HypaRNP-modified bands. Percentage of indel mutation was quantified using ImageLab. *p*-values compared to untreated control are denoted as * and ** for $p \leq 0.05$ and $p \leq 0.01$, respectively. Scale bar, 20 μm.

Solution SAXS Measurements: SAXS measurements were performed at Pohang Accelerator Laboratory, 4C SAXS II beamline (BL4C, PAL, Korea). A light source from an In-vacuum Undulator 20 (IVU20: 1.4 m short, 20 mm period) of the Pohang Light Source II storage ring yielded an X-ray beam wavelength of 0.73 Å. The magnitude of scattering vector, $q = (4\pi/\lambda) \sin\theta$, was 0.070 $nm^{-1} < q < 1.2$ nm^{-1}, where 2θ is the scattering angle and λ is X-ray beam the wavelength. X-ray diffraction data were collected in capillary cells, at 4 °C, with 4.0 m of sample-to-detector distance. SAXS patterns were collected for six successive frames of 5 s exposure to monitor radiation damage. Final scattering data were generated by subtracting with control and merging data from all concentrations. The pair distribution function $P(r)$ was calculated using the Fourier inversion of the scattering intensity $I(q)$. The molecular masses of samples were determined using BSA scattering as a standard. Detailed SAXS data and analysis statistics are summarized in Table S4 (Supporting Information).

Target DNA Cleavage and Indel Mutation Assay: The DNA duplex substrate was amplified and purified from the PCR product of eGFP gene. The Cas9:sgRNA RNP complex was purified using a size exclusion column. Reaction was conducted by mixing the DNA substrate and RNP (ratio 1:10) in buffer C (20×10^{-3} M Hepes-NaOH, pH 7.4, 150×10^{-3} M NaCl, 5×10^{-3} M MgCl2, 0.1×10^{-3} M EDTA, 5% glycerol, 5 μg mL^{-1} BSA) for 30 min at 37 °C. The reaction was quenched by adding proteinase K (1 mg mL^{-1}) at room temperature for 20 min. The cleavage products were fractionated using 2% agarose gel electrophoresis. For analysis of indel mutation frequency, the T7E1 assay was performed. Genomic DNA from human cells was extracted using the genomic DNA isolation kit (Invitrogen, MA, USA). The eGFP gene was amplified from genomic DNA using Q5 fidelity DNA polymerase (NEB, MA, USA) and specific set of primers (Table S1, Supporting Information). After denaturation and annealing of the PCR product, the sample was digested with T7E1 (Toolgen, Korea) for 20 min at 37 °C per manufacturer's instructions.

The digestion product was separated and visualized using 2% agarose gel electrophoresis and staining with safe SYBR (Thermo Scientific, USA). Subsequently, the bands were quantified to obtain the gene modification frequencies mediated by the CRIPSR/Cas9 system using ImageLab (Chemidoc, Biorad, USA) per the following formula: frequency (%) = [1 − (cleaved fractions/total)] × 100. Experiments were conducted in triplicate. The primers used for amplification and the guide RNA sequence are shown in Table S1 (Supporting Information).

Supporting Information

Supporting Information is available from the Wiley Online Library or from the author.

Acknowledgements

The authors thank the staff at the SAXS beamline 4C-SAXSII (Pohang Light Source, Korea) for technical assistance. This work was supported by the Institute for Basic Science (IBS-R015-D1), Korea Institute of Science and Technology (KIST-2E29563-19-119), IMNEWRUN CORPORATION, and the Basic Science Research Program through the National Research Foundation of Korea (NRF), which is funded by the Ministry of Education (NRF-2017R1A1B0306021).

Conflict of Interest

The authors declare no conflict of interest.

Keywords

delivery, dNP2 lipopeptides, gene editing, hyper-accurate Cas9, nanosomes

Received: June 19, 2019
Revised: September 16, 2019
Published online: October 7, 2019

[1] a) T. Wang, J. J. Wei, D. M. Sabatini, E. S. Lander, *Science* **2014**, *343*, 80; b) V. Singh, D. Braddick, P. K. Dhar, *Gene* **2017**, *599*, 1; c) L. A. Marraffini, in *Streptococcus Pyogenes: Basic Biology to Clinical Manifestations* (Eds.: J. J. Ferretti, D. L. Stevens, V. A. Fischetti), University of Oklahoma Health Sciences Center, Oklahoma City (OK) **2016**.

[2] a) J. L. Gori, P. D. Hsu, M. L. Maeder, S. Shen, G. G. Welstead, D. Bumcrot, *Hum. Gene Ther.* **2015**, *26*, 443; b) M. A. DeWitt, J. E. Corn, D. Carroll, *Methods* **2017**, *121–122*, 9.

[3] a) B. P. Kleinstiver, V. Pattanayak, M. S. Prew, S. Q. Tsai, N. T. Nguyen, Z. Zheng, J. K. Joung, *Nature* **2016**, *529*, 490; b) A. A. Dominguez, W. A. Lim, L. S. Qi, *Nat. Rev. Mol. Cell Biol.* **2016**, *17*, 5.

[4] a) E. Oude Blenke, M. J. Evers, E. Mastrobattista, J. van der Oost, *J. Controlled Release* **2016**, *244*, 139; b) Y. Fu, J. A. Foden, C. Khayter, M. L. Maeder, D. Reyon, J. K. Joung, J. D. Sander, *Nat. Biotechnol.* **2013**, *31*, 822; c) C. A. Lino, J. C. Harper, J. P. Carney, J. A. Timlin, *Drug Delivery* **2018**, *25*, 1234.

[5] a) R. Mout, M. Ray, G. Yesilbag Tonga, Y. W. Lee, T. Tay, K. Sasaki, V. M. Rotello, *ACS Nano* **2017**, *11*, 2452; b) J. A. Zuris, D. B. Thompson, Y. Shu, J. P. Guilinger, J. L. Bessen, J. H. Hu, M. L. Maeder, J. K. Joung, Z. Y. Chen, D. R. Liu, *Nat. Biotechnol.* **2015**, *33*, 73; c) S. Kim, D. Kim, S. W. Cho, J. Kim, J. S. Kim, *Genome Res.* **2014**, *24*, 1012.

[6] M. Jinek, F. Jiang, D. W. Taylor, S. H. Sternberg, E. Kaya, E. Ma, C. Anders, M. Hauer, K. Zhou, S. Lin, M. Kaplan, A. T. Iavarone, E. Charpentier, E. Nogales, J. A. Doudna, *Science* **2014**, *343*, 1247997.

[7] K. Lee, M. Conboy, H. M. Park, F. Jiang, H. J. Kim, M. A. Dewitt, V. A. Mackley, K. Chang, A. Rao, C. Skinner, T. Shobha, M. Mehdipour, H. Liu, W. C. Huang, F. Lan, N. L. Bray, S. Li, J. E. Corn, K. Kataoka, J. A. Doudna, I. Conboy, N. Murthy, *Nat. Biomed. Eng.* **2017**, *1*, 889.

[8] W. Zhou, H. Cui, L. Ying, X. F. Yu, *Angew. Chem.* **2018**, *57*, 10268.

[9] S. K. Alsaiari, S. Patil, M. Alyami, K. O. Alamoudi, F. A. Aleisa, J. S. Merzaban, M. Li, N. M. Khashab, *J. Am. Chem. Soc.* **2018**, *140*, 143.

[10] a) I. W. Hamley, *Chem. Commun.* **2015**, *51*, 8574; b) C. Dutta, K. Chakraborty, R. Sinha Roy, *ACS Appl. Mater. Interfaces* **2015**, *7*, 18397.

[11] a) S. Lim, W. J. Kim, Y. H. Kim, S. Lee, J. H. Koo, J. A. Lee, H. Yoon, D. H. Kim, H. J. Park, H. M. Kim, H. G. Lee, J. Yun Kim, J. U. Lee, J. Hun Shin, L. Kyun Kim, J. Doh, H. Kim, S. K. Lee, A. L. Bothwell, M. Suh, J. M. Choi, *Nat. Commun.* **2015**, *6*, 8244; b) M. Li, K. Shi, X. Tang, J. Wei, X. Cun, X. Chen, Q. Yu, Z. Zhang, Q. He, *Eur. J. Pharm. Sci.* **2018**, *124*, 240.

[12] a) A. Erazo-Oliveras, N. Muthukrishnan, R. Baker, T. Y. Wang, J. P. Pellois, *Pharmaceuticals* **2012**, *5*, 1177; b) H. C. Christianson, M. Belting, *Matrix Biol.* **2014**, *35*, 51.

[13] J. S. Chen, Y. S. Dagdas, B. P. Kleinstiver, M. M. Welch, A. A. Sousa, L. B. Harrington, S. H. Sternberg, J. K. Joung, A. Yildiz, J. A. Doudna, *Nature* **2017**, *550*, 407.

[14] L. A. Kelley, S. Mezulis, C. M. Yates, M. N. Wass, M. J. Sternberg, *Nat. Protoc.* **2015**, *10*, 845.

[15] W. L. DeLano, *The PyMOL Molecular Graphics System*, DeLano Scientific LLC, San Carlos, CA **2002**.

[16] a) J. A. Doudna, E. Charpentier, *Science* **2014**, *346*, 1258096; b) F. Jiang, J. A. Doudna, *Annu. Rev. Biophys.* **2017**, *46*, 505.

[17] S. Ramakrishna, A. B. Kwaku Dad, J. Beloor, R. Gopalappa, S. K. Lee, H. Kim, *Genome Res.* **2014**, *24*, 1020.

[18] a) H. X. Wang, Z. Song, Y. H. Lao, X. Xu, J. Gong, D. Cheng, S. Chakraborty, J. S. Park, M. Li, D. Huang, L. Yin, J. Cheng, K. W. Leong, *Proc. Natl. Acad. Sci. USA* **2018**, *115*, 4903; b) S. Ramakrishna, S. W. Cho, S. Kim, M. Song, R. Gopalappa, J. S. Kim, H. Kim, *Nat. Commun.* **2014**, *5*, 3378.